Modelling the effect of myosin X motors on filopodia growth

K Wolff[1,2,4]**, C Barrett-Freeman**[2,4]**, M R Evans**[2]**, A B Goryachev**[3]
and D Marenduzzo[2,5]

[1] Institut für Theoretische Physik, Technische Universität Berlin, Hardenbergstraße 36, D-10623 Berlin, Germany
[2] SUPA, School of Physics and Astronomy, University of Edinburgh, Mayfield Road, Edinburgh EH9 3JZ, UK
[3] Centre for Systems Biology, School of Biological Sciences, University of Edinburgh, Mayfield Road, Edinburgh EH9 3JR, UK

E-mail: katrin.wolff@tu-berlin.de and dmarendu@ph.ed.ac.uk

Abstract
We present a numerical simulation study of the dynamics of filopodial growth in the presence of active transport by myosin X motors. We employ both a microscopic agent-based model, which captures the stochasticity of the growth process, and a continuum mean-field theory which neglects fluctuations. We show that in the absence of motors, filopodia growth is overestimated by the continuum mean-field theory. Thus fluctuations slow down the growth, especially when the protrusions are driven by a small number (10 or less) of F-actin fibres, and when the force opposing growth (coming from membrane elasticity) is large enough. We also show that, with typical parameter values for eukaryotic cells, motors are unlikely to provide an actin transport mechanism which enhances filopodial size significantly, unless the G-actin concentration within the filopodium greatly exceeds that of the cytosol bulk. We explain these observations in terms of order-of-magnitude estimates of diffusion-induced and advection-induced growth of a bundle of Brownian ratchets.

S Online supplementary data available from stacks.iop.org/PhysBio/11/016005/mmedia

---

1. Introduction

Cell motility is a fascinating and intricate process [1, 2]. Largely, cell motion is driven by the dynamics of the actin cytoskeleton, a network of semiflexible polymers—the actin fibres—interacting with molecular motors and with a number of actin-binding proteins [2]. Actin fibres grow at one of their ends, called the plus or barbed end, and shrink at the other, known as the minus or pointed end. At least when cells crawl on a 2D substrate, the mechanism through which they move is well understood. A simplified view is that the growth of actin fibres at the barbed end pushes the membrane forward, while the contractility due to myosin motors, which are mainly at the back, ensures that the cell body is dragged along [1].

In a more detailed description, crawling proceeds via the rectification of Brownian fluctuations in the membrane by actin polymerization [3]. For this to be a viable motility protocol, there has to be sufficient 'friction' with the substrate for the growing fibres to be able to push without slipping behind. In physiological conditions this required friction is provided by focal adhesions i.e. protein clusters which attach the cell to the substrate [4]. Such structures are likely to be absent in three-dimensions (3D), and it has been proposed that contractility may have a more primary role in initiating and sustaining 3D cell motility, e.g. within a tissue [5–7].

When a cell crawls on a substrate, it does so by protruding a flat sheet of material packed with growing actin filaments: this quasi-2D structure is known as the *lamellipodium* [1, 8]. While the lamellipodium is arguably the best documented structure in crawling cells, there are a number of other important actin-driven protrusions, such as actin ruffles,

---

[4] These authors contributed equally to this work.
[5] Author to whom any correspondence should be addressed.

pseudopodia, podosomes and filopodia [9–19]. We will be in particular concerned with the latter in the current work. Filopodia are fingerlike protrusions of the cell which are thought to be engaged in exploratory cell movements, e.g. to sense the external environment prior to lamellipodium-associated motion [1]. They are formed by bundles of actin fibres, which extend and retract due to actin polymerizing and de-polymerizing at the ends of the fibres in these bundles. The fibre tips are protected against capping (which would halt growth, or extension, of the filopodium) by cytosolic proteins. The growth of the actin fibres is instead limited by slow transport of monomeric actin to the tip of the filopodium, and eventually by membrane elasticity which resists the large deformation associated to the formation of these protrusions.

There have been a number of studies on the physics of filopodia in recent years [11, 14–19]. Mogilner and Rubinstein proposed a mean-field theory to study filopodia dynamics in a seminal paper [11], and Monte Carlo simulations of varying levels of complexity have been implemented [16, 19] to assess the role of fluctuations and of actin-binding proteins. Here we study the growth of filopodia via actin polymerization in two different frameworks. In the first, we assume that the growth is driven solely by the diffusion of monomeric G-actin to the tip of the filopodium. In the second scenario, following recent work in [15, 17, 18] we explore the possibility that myosin X motors, which are known to be enriched at the tip of growing filopodia, enhance the transport of monomeric G-actin to the tip. One might expect that this second transport scenario would lead to much faster growth of the filopodium, because transport by advection should be, at least for large times, much more efficient than unbiased diffusion. As was suggested in [15] with a microscopic agent-based model, and as we show here by numerically simulating a continuum set of equations, this turns out not to be the case.

In this paper we work on both a microscopic and a coarse-grained level by using, respectively, an agent-based model and a set of continuum equations of motion. We compare the two frameworks, both qualitatively and quantitatively, and identify key differences in their predictions. Our main new results are as follows.

First, we find that when the force opposing growth (which comes from membrane elasticity) is large (10 pN or more), then the mean-field approach significantly overestimates the growth rate of filopodia. This is mainly due to the mean-field theory's failure to capture correlations between successive polymerization events at large force, as we show by analysing a simpler model where the concentration of G-actin is uniform. This result is important as it points to potentially significant limitations of mean-field theory when used to describe a bundle of Brownian ratchets, an approach which is often followed in the literature.

Second, our results suggest that, given commonly used parameters for actin transport and filopodia dynamics, motors are unlikely to be able to speed up the growth of such protrusions by simply delivering actin monomers through advection. To reach our conclusions we use a continuum theory which predicts the growth dynamics of filopodia by coupling the Brownian ratchet dynamics to the diffusion and advection

of G-actin monomers to the filopodium tip. This complements previous work on the same topic [15] which arrived at similar conclusions using agent-based simulations. We also explain these seemingly counterintuitive results on the basis of simple order-of-magnitude estimates for the diffusion and advection induced growth laws.

Finally, we critically assess how our results may be changed if some of our assumptions are modified. For instance we find that, if one were to assume that the diffusion of actin monomers in the narrow tube making up a filopodium were significantly slower than the bulk diffusion (an order of magnitude), then unbiased diffusion would become a serious bottleneck for filopodial growth. In that case motor-driven advection could help to overcome the bottleneck. Potentially, advection could also become relevant if the G-actin concentration within the filopodium greatly exceeded that of the cytosol bulk, suggesting that experiments aimed at determining that concentration would be very valuable to make further progress theoretically.

The paper is structured as follows. In section 2.1 we introduce the model, in section 2.2 we describe the agent-based microscopic description of the filopodium dynamics, whereas in section 2.3 we outline our continuum model, which is based on a set of partial differential equations. We then discuss the results obtained by our models in section 3, starting from the case where the tip of the actin bundle within the filopodium grows solely due to the free diffusion of actin from the bulk of the cell, and then assess the relevance of potential actin monomer transport by advection through the action of myosin motors. Finally, our conclusions are presented in section 4.

2. Model and methods

2.1. The model

The system we consider is a growing filopodium, enclosed within, and pushing against, a cylindrical cell membrane (radius r_{cyl}, see cartoon in figure 1). The filopodium is a bundle of N actin fibres, each of which is assumed to be infinitely stiff[6] The tip of the filopodium extends via the polymerization of monomeric, or G-actin, into filamentous, or F-actin. Monomeric actin can either reach the tip by diffusing within the cytosol, or, potentially, it can be recruited there through directed transport by myosin X motors. The motors are associated with the filopodium and we consider them to move uniformly along the filaments at a constant velocity v (we therefore do not directly model motors). In our framework, G-actin monomers, in addition to diffusion, can attach and detach from the bundle (at rate k_a and k_d respectively). When they are attached, they are transported towards the tip by myosin X. Finally, the top of the cell membrane diffuses and is subject to a load (a force f, which *in vivo* comes from elastic deformation of the membrane and viscous drag).

---

[6] As the persistence length of a single actin fibre is about 17 μm [20], one should note that a force of only a few pN would be enough to buckle a single actin fibre of size 100 nm. Nevertheless our approximation of using infinitely stiff fibres is here justifiable as the persistence length of an actin bundle is much larger than that of a single fibre; it may scale as the number of fibres square if these are appropriately crosslinked [11, 14].
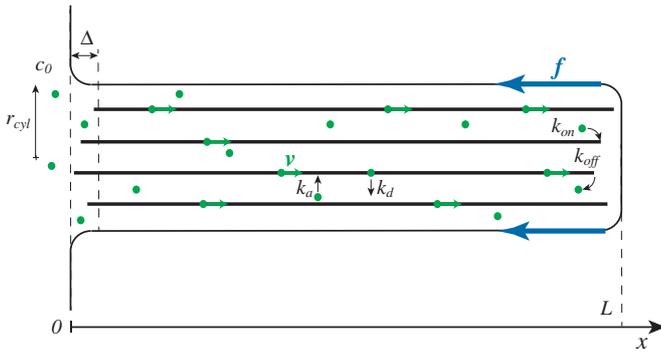
Figure 1. Sketch of our model for the growing filopodium inside a cylindrical membrane (whose top, on the right, undergoes Brownian motion against an external load f). Symbols are defined in the text in sections 2.1 and 2.2.

Table 1. Model parameters.

Symbol	Meaning	Value	Reference
r_{cyl}	Radius of filopodium	100 nm	[25]
N	Number of fibres	$\sim$10–30	[11]
f	Membrane resistance force	$\sim$10–50 pN	[11]
$k_B T$	Thermal energy	4.1 pN nm	[3]
δ	Actin monomer half-width	2.7 nm	[3]
D	G-actin diffusion constant	$\sim$5 μm^2 s^{-1}	[26]
D_m	Membrane diffusion constant	$\sim\mathcal{O}(1)$ μm^2 s^{-1}	
c_0	G-actin concentration in the cell body	10 μM	[11]
k_{on}	Polymerization rate	10 μM^{-1}s^{-1}	[27]
k_{off}	De-polymerization rate at tip	$\simeq$1 s^{-1}	[24]
v_{retr}	Retrograde flow velocity	10–30 nm s^{-1}	[28]
η	Geometric conversion coefficient	18.9 μM^{-1} μm^{-1}	[11]

2.2. Agent-based simulations

In this section we describe a microscopic agent-based simulation of the model for growth of a filopodium just outlined. This approach is useful as it can include a relatively high level of detail, and, importantly, it incorporates fluctuations in the G-actin density. Our purpose will be to compare these agent-based simulations to a simplified, and computationally cheaper, mean-field approach.

In the agent-based simulations we explicitly model G-actin monomers diffusing freely in the 3D space within the filopodial protrusion. This is done by attempting, at every time step, to displace monomers randomly by a distance chosen uniformly between $-\delta l$ and δl along each dimension. The resulting diffusion coefficient is equal to $\delta l^2/(6\delta t)$ (see e.g. [21]), where δt is the time step. In the simulation, the monomers are taken to be point particles (in other words we neglect the steric interactions between two G-actin monomers or between a G-actin monomer and an F-actin filament).

The filopodial protrusion is assumed to be cylindrical with constant radius r_{cyl} and a flat top. Monomers can enter and leave this cylinder only via the base. At the base, the G-actin concentration is held constant at the bulk value c_0 ($\sim$10 μM, see table 1)[7], while there are no flux boundary conditions on the lateral and top surfaces of the cylindrical filopodium.

A G-actin monomer that diffuses up to the leading edge of the filopodium can polymerize to become F-actin, if there is a large enough gap between the fibre tip and the top membrane. In order for polymerization to occur, the distance between the G-actin monomer and the tip of one of the F-actin filaments must be smaller than an appropriate 'polymerization radius' (similar concepts arise when simulating stochastic chemical reactions, see [22]). We also introduce a probability of polymerization, with which a G-actin monomer within the polymerization range becomes part of the extending F-actin filament. The polymerization radius and probability are calibrated so as to give a steady-state polymerization rate, for a fixed G-actin concentration within the filopodium, in agreement with the experimental rate of $k_{on} = 10\,\mu$M^{-1}s^{-1}. This is ensured by choosing a polymerization radius $\delta_{pol} = 0.5$ and a polymerization probability $p_{pol} = 0.00917$ (both in simulation units).

The top membrane of the protrusion also diffuses. To simulate this stochastic membrane motion we postulate that the top undergoes a random walk against an opposing force f which represents elastic restoring forces. We use the Metropolis algorithm [23], so that we always accept trial membrane displacements towards the cell body (as long as they are not impeded by fibres of the filopodium) but only accept membrane displacements away from the cell body with probability $\exp(-f|\Delta x|/k_B T)$, where Δx is the displacement along the positive x direction. The opposing force takes a value $f \sim$10–50 pN, estimated e.g. in [11]. Our agent-based simulations essentially follow a kinetic Monte Carlo scheme, which disregards hydrodynamic interactions. Monomers and membrane therefore diffuse independently and there is no dragging of monomers due to the moving boundary. This is justified by the negligible effects of the flow field, v, due to the moving membrane compared with the diffusion of actin monomers (as the Peclet number $v\sigma/D \ll 1$, where σ and D are the G-actin size and diffusion coefficient respectively).

At the growing tip of the filopodium we also model F-actin depolymerization: at a rate $k_{off} \simeq 1$ s^{-1} (realistic *in vivo* [24]) the last actin monomer turns into diffusing G-actin.

We simulate only the growth of filopodia, not the first emergence of protrusions from the cell body, and therefore start filopodia at a finite length of L_{start}. Finally, we model the retrograde flow by retracting the fibres by one F-actin monomer every fixed number of time steps thereby losing one actin monomer from the base.

As for length and time scales in the simulations, we use the G-actin monomer width of $\Delta x = 5.4$ nm to set our simulation length scale[8]. The time scale is set by the 'Brownian time' over which G-actin diffuses its own size, $\tau = \Delta x^2/(6D)$, where the diffusion constant is $D = 5\,\mu$m^2 s^{-1}. We choose a simulation time step of $\Delta t = 0.04\,\tau$. An overview of the model parameters and references can be found in table 1. Note that to simulate membrane diffusion we use a maximum step size equal to 0.1 (in simulation units), corresponding to a diffusion coefficient $D_m = 1.25\,\mu$m^2 s^{-1}. This value is reasonable for an object of the size of the filopodium diameter,

---

7 This boundary condition requires inspection of the local concentration at the base, and injection of monomers when this concentration falls below c_0.

8 Because of the way the actin monomers are stacked in the actin fibre, this only grows by $\delta = 2.7$ nm $= 0.5\,\Delta x$ upon addition of a G-actin monomer.

in an aqueous (rather than an intracellular) environment. In reality, the effective viscosity of the medium into which the filopodium grows may well be larger; however, our results are qualitatively unchanged provided that membrane diffusion remains fast with respect to actin polymerization. This is true if the dimensionless ratio $c(L) k_{on} \delta^2 / D_m \ll 1$ at all times, where $c(L)$ is the G-actin concentration at the tip. This condition is realistic for filopodia under physiological conditions. Moreover, the condition is necessary for the ratchet equations [3] to hold.

Our filopodium is made up of a bundle of static rigid fibres, and for simplicity these are imagined to be anchored to the underlying cytoskeletal mesh, so that the origin of the filaments does not move[9]. Therefore, in principle, it matters where each fibre is initially positioned with respect to the base of the filopodium. Placing all the fibres in exact alignment leads to stalling at an artificially small value of the force, because all fibres in the bundle 'lock' at the same distance from the membrane top and the membrane would have to be displaced by an entire monomer half-width to allow polymerization. This is unphysical as in reality the actin filaments can displace and bend to accommodate growth at the end [29–31]. To overcome this problem, we placed the fibres within a distance Δ of the base. We found that spacing the fibre roots uniformly in $[0, \Delta]$ and choosing $\Delta = \delta$, the size of the increment of an F-actin filament, leads to the fastest growth, therefore, we have chosen these settings. This choice of parameters reproduces the stalling force predicted by the mean-field continuum model which we discuss below. Positioning the fibres randomly leads to the same stalling force, and to qualitatively similar results as the ones reported below, although the growth rate is quantitatively lower.

2.3. Continuum mean-field equations

In this section we introduce a continuum model to which the agent-based simulations may be compared. We propose the following set of partial differential equations for the dynamics of a growing filopodium:

$$\frac{\partial c_a}{\partial t} = -v\frac{\partial c_a}{\partial x} + Nk_a c_d - k_d c_a \tag{1}$$

$$\frac{\partial c_d}{\partial t} = D\frac{\partial^2 c_d}{\partial x^2} - Nk_a c_d + k_d c_a \tag{2}$$

$$\frac{\partial L}{\partial t} = \delta \left[k_{on} e^{-\beta f \delta / N} c_d(L) + \frac{v c_a(L)\eta}{N} e^{-\beta f \delta / N} - k_{off} \right] - v_{retr} \tag{3}$$

where $c_a(x, t)$ is the concentration of advected G-actin, $c_d(x, t)$ is the concentration of diffusing G-actin and L is the filopodium length. We note that similar equations have appeared in [11, 16, 17], although the coupling between ratchet dynamics and simultaneous advection and diffusion of G-actin is new to our approach.

---

[9] We expect that allowing fibres to diffuse under the action of a spring which links them to their origin (to mimic entanglement or attachment to the cytoskeletal mesh) will not change our main results qualitatively. This is supported by selected simulations within the simplified model of section 3.2.

The first, equation (1), represents the advective transport of G-actin and v is the motor-induced advection velocity along the filopodium. The second and third terms on the right-hand side of equation (1) represent attachment of free G-actin to each of the N fibres with rate k_a and unbinding of attached G-actin with rate k_d. The factor Nk_a reflects the fact that diffusing actin can attach to a motor on each of the N fibres in the bundle.

Equation (2) represents the diffusive transport of free G-actin, where D is the diffusion coefficient of free G-actin in the cytosol. Again, the second and third terms on the right-hand side represent attachment of free G-actin and unbinding of attached G-actin.

The last of the equations (equation (3)), is the ratchet equation for filopodium growth. The terms in the square brackets represent growth and shrinkage from processes at the tip whereas the term $-v_{retr}$ represents shrinkage due to the filopodium retrograde flow. At the filopodium tip, k_{on} and k_{off} are the on and off polymerization rates for the interaction between G-actin and the filopodium actin filaments (which are assumed to be uniformly covered with myosin X motors) and $v c_a(L)\eta$ is the polymerization rate from advected G-actin. For convenience, we write the latter rate in terms of η, a dimensional factor, equal to $\sim 18.9 \, \mu M^{-1} \mu m^{-1}$ [11], which transforms densities per unit volume into densities per unit length of the filopodium. The polymerization rate k_{on} and $v c_a(L)\eta$ are multiplied by the Boltzmann factor $e^{-\beta f \delta / N}$, $\beta = \frac{1}{k_B T}$, with k_B the Boltzmann constant and T the temperature, and $f\delta/N$ is the energy cost of extension against the constant opposing force f of the resisting membrane. We take δ, the size of the increment of an F-actin filament, to be equal to 2.7 nm, half the size of a G-actin monomer. Note that in the ratchet equation for $L(t)$, equation (3), the increase in the length of the filopodium comes from two separate additive terms that correspond to the diffusing and advected populations. While the first term which comes from diffusion is standard [11], the second, advection contribution is new—note that the increase due to advection is inversely proportional to the number of fibres, as we need N advected monomers to increase the whole filopodial length by the size of an actin monomer. The advection contribution follows from assuming that monomers extend the filopodium as soon as they are advected to the tip. In principle one might include a reaction rate for this process, but this would not qualitatively affect our results. We also highlight at this point the mean field 'load sharing' approximation in equation (3), according to which the growth of a bundle can be written by mapping $k_{on,off} \rightarrow Nk_{on,off}$, $\delta \rightarrow \delta/N$ in the equation valid for a single fibre [11, 12, 14]. As we shall see, this approximation may lead to discrepancies between the continuum theory and the agent-based simulations. We will further discuss this fact in section 3.2.

We consider the following boundary conditions:

$$c_a(x = 0, t) + c_d(x = 0, t) = c_0 \tag{4}$$

$$\frac{c_a(x = 0, t)}{c_d(x = 0, t)} = \frac{Nk_a}{k_d} \tag{5}$$

$$-\left[\frac{D\partial c_d(x,t)}{\partial x}\right]_{x=L(t)} = \frac{N}{\eta}[k_{\text{on}}c_d(L)e^{-\beta f\delta/N} - k_{\text{off}}], \qquad (6)$$

where c_0 is the bulk concentration of G-actin, 10 μM.

At $x = 0$, i.e. at the base of the filopodium, boundary condition (5) states that the advected and freely diffusing populations are in equilibrium and boundary condition (4) states that the total density is the typical bulk concentration of G-actin. This choice of boundary conditions has previously been made in the literature in [15], where it was argued that this boundary condition is most consistent with existing experimental data. An alternative choice of boundary condition would be to fix $c_d(0)$, rather than $c_d(0) + c_a(0)$, to c_0, and to take $c_a(0)$ to be proportional to N, as more filaments provide more binding sites. However, this would also require the G-actin density in filopodia to be several-fold larger than in the bulk, a fact which has not been reported to date to our knowledge. This alternative choice of boundary condition *would* modify our conclusions and we will discuss it again in section 3.4 when we comment on the implications of our results for the growth of filopodia in presence of myosin X motors, but we believe it to be less realistic than the boundary conditions in equations (4) and (5).

On the other hand, the boundary condition equation (6) at $L(t)$, i.e. at the tip of the filopodium, states that there is a sink for the diffusing G-actin, due to polymerization. This sink term is formally the same as the purely diffusive term proposed in the previous work [11, 15], which comes from our assumption (discussed above) that the exit flux of advected actin at the tip of the filopodium is $ve^{-\beta f\delta/N}c_a(L)$ (hence drops out of the equation for the diffusing G-actin sink).

Note that we do not include any exclusion interaction between the motors. The exclusion interaction has revealed interesting properties in a number of molecular motor systems on dynamic filaments e.g. fungal hyphal growth [32], elongating actin filaments [33] and extraction of membrane tubes by motors [34]. In principle, we could include exclusion by turning the advection equation into a Burgers equation with a reaction term—as was incorporated in recent work on filopodia [17] for the density profiles of motors on actin filaments. Our choice to not model exclusion is justified in our context as its effects would only be important if the concentration of bound monomer were as high as 1 per filament per 5 nm (corresponding to 50% of the filopodial length being associated with advected G-actin). This requires, for a filopodium made up of ten fibres, a 200 μM concentration of G-actin, which is far above the typical bulk G-actin concentration (around 10 μM) considered in our calculations.

Finally, we note that we can estimate the maximal length of the filopodium from the above equations, under the assumption that there is no advection (we follow exactly the same procedure used in [16], repeating the intermediate steps for the reader's convenience). We assume that the density profile in the steady state will be a linearly decreasing function of x, and the gradient can therefore be reasonably approximated by:

$$\frac{\partial c}{\partial x} \simeq \frac{c(L) - c_0}{L}. \qquad (7)$$

(This assumption is backed up by observations of density profiles in numerical simulations of equations (1) and (3).) We then use the boundary condition at the tip to derive an expression for the actin concentration there, $c(L)$:

$$c(L) = \frac{LNk_{\text{off}} + c_0D\eta}{D\eta + LNk_{\text{on}}\exp(-f\delta/Nk_BT)}. \qquad (8)$$

Substituting this result into the equation for $L(t)$ and requiring $dL/dt = 0$ yields the steady state, or maximal, length:

$$L_{\text{max}} = \frac{D\eta}{Nk_{\text{on}}}\left[\frac{\delta k_{\text{on}}c_0}{v_{\text{retr}}} - \left(\frac{\delta k_{\text{off}}}{v_{\text{retr}}} + 1\right)e^{\frac{f\delta}{Nk_BT}}\right]. \qquad (9)$$

Using the values in table 1, we find the maximal length to be ~ 1–$10\,\mu$m.

3. Results

3.1. Filopodia growth in the absence of motors: comparison between agent-based and continuum models

In this section we compare the results obtained from numerical integration of equations (1)–(3) (which we refer to as the continuum mean-field theory), with those from agent-based simulations in the absence of motors. This will help to understand whether the mean-field model is a good approximation for the system it attempts to describe and, if so, what ranges of parameters it works well for. To this end, we compare the filopodium growth (lengths as a function of time) obtained with the two methods. In general, as we will show below, the agreement is qualitatively good, at least for physiological values of the parameters. There are however significant quantitative differences which we will also address.

As should be expected, the agreement between agent-based simulation and the continuum mean-field theory is best for a large number of fibres N (see figure 2). This is due to the effect of fluctuations, neglected in the mean-field continuum approach, which are more significant for a small number of fibres. Both the mean-field theory and the agent-based simulations predict that the filopodium grows faster for an intermediate number of fibres (see figure 2 where the bundle of $N = 10$ fibres grows faster than that with $N = 1$ or $N = 30$). This non-monotonic behaviour can be explained intuitively by noting that for a large number of filaments the bundle needs more actin monomers to fuel its growth. On the other hand, growth is considerably reduced in the case of very few fibres as the bundle is more sensitive to the action of the external force: this effect enters through the factor of f/N in the Boltzmann factor in the ratchet equation in equation (3) (see also [11, 12, 14]).

Next, we investigate the effect of varying the membrane force f at a fixed number of fibres $N = 30$ (a reasonable assumption for typical filopodia *in vivo* [9, 11]). For small values, $f = 1$–5 pN, the hindering of growth is rather minimal, in both the mean-field and the agent-based model. When $f = 5$ pN, the agent-based simulation begins to be affected and growth is reduced. We find that the agent-based model is affected by increasing force more strongly than the mean-field model, leading to a marked discrepancy between the two approaches (see figure 3).
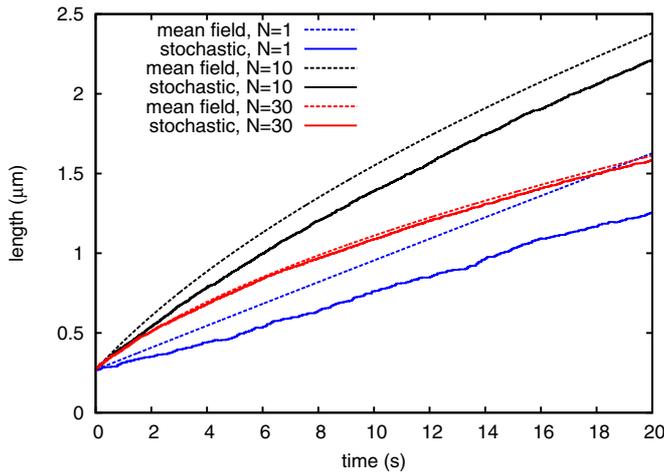
Figure 2. Comparison of agent-based (solid lines) and mean-field (dashed lines) simulations, in the absence of advection by molecular motors. The only transport channel for G-actin is through unbiased diffusion. Membrane resistance force is $f = 2$ pN, concentration $c_0 = 10 \, \mu$M, depolymerization rate $k_{off} = 1 \, s^{-1}$. The number of the filaments in the bundle is varied (see legend). The mean-field approximation improves for larger values of N, for which stochastic fluctuations are less important. The data also show that there should be an optimum number of filaments at fixed monomer concentration—10 fibres grow faster than either 30 or a single filament. This result is fully consistent with the findings in [11], which were obtained with a continuum mean-field theory.
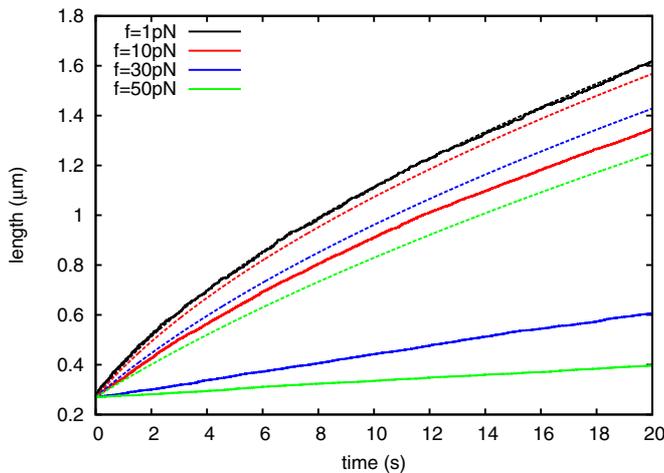

Figure 3. Comparison of agent-based (solid lines) and mean-field (dashed lines) simulations, in the absence of advection by myosin motors. The number of filaments is fixed at $N = 30$, while the concentration of G-actin in the bulk (at the base of the filopodium) is $c_0 = 10 \, \mu$M, and the depolymerization rate is $k_{off} = 1 \, s^{-1}$. The membrane resistance force is varied. The mean-field approximation gets worse for increasing force, where it severely underestimates the slowing down induced by the external force.

Increasing the force further decreases the growth rate until the stalling force is reached. The prediction for the stalling force with $N = 30$ is given by equation (3) as $f_s = 210$ pN and both the continuum model solution and the microscopic dynamics agree on this. The greater sensitivity of the growth rate on the applied force in the agent-based simulation is due to the mean-field approximation implicit in the ratchet equation (3) i.e. in going from a ratchet equation for a single
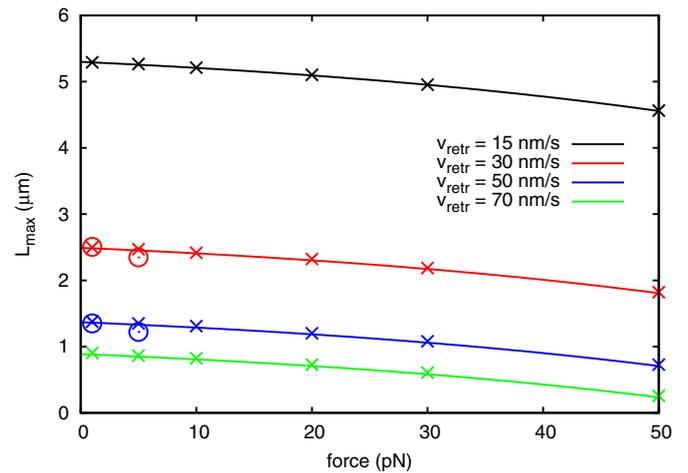

Figure 4. Steady-state filopodium length as a function of membrane resistance force from analytic prediction (solid lines), numerical integration of the mean-field continuum equations (crosses) and agent-based simulations (open circles) for various values of the membrane resistance, $f = 1.0, 5.0, 10.0, 20.0, 30.0, 50.0$ pN. The retrograde flow rate is also varied $v_{retr} = 15, 30, 50, 70$ nm s^{-1}. Other simulation parameters are $N = 30$, $k_{off} = 1 \, s^{-1}$ and $c_0 = 10 \, \mu$M.

filament to an equation for a bundle of N filaments we have simply replaced $\delta \to \delta/N$, $k_{on} \to Nk_{on}$ and $k_{off} \to Nk_{off}$ (see also [11, 12, 14]). This point will be discussed further in section 3.2.

Increasing bulk concentration c_0 speeds up the growth (data not shown), as would be expected, but has little effect on the agreement between the mean-field theory and the microscopic simulation.

Up to now we have neglected the retrograde flow, v_{retr} (see sections 2.1 and 2.2). This is not realistic as in practice actin polymerization is always accompanied by a retrograde flow of the network [35]. If we now introduce a non-zero v_{retr}, we find that the system can reach a steady state as expected from the analysis of the continuum equation without the advection proposed above (and paralleling that in [11]). For small values of the retrograde flow, ~ 10 nm s^{-1} (typically quoted in experiments, see e.g. [35]), the continuum model predicts that the system should take about 1000 s to reach a steady state. For greater values, such as $v_{retr} = 70$ nm s^{-1}, employed in [11, 16] to describe filopodia emerging from a lamellipodium, the steady state would be attained an order of magnitude sooner. In figure 4, we compare the approximate steady-state solution found in section 2.2, see equation (9), with the steady-state lengths found by direct numerical simulation of the mean-field equations—the estimate and the exact value are in excellent agreement. We also simulated growth in the agent-based model with retrograde flow (open symbols in figure 4). The results reinforce our main previous finding, that for larger forces the continuum model overestimates growth rates (figure S1, available at stacks.iop.org/PhysBio/11/016005/mmedia) and also, in this case, steady-state lengths.

In this section we have seen that the agreement between the agent-based model and numerical simulation of the mean-field model is reasonably close for realistic parameter values. For small numbers of actin filaments the discrepancy

between the models grows (as expected) but qualitatively the predictions still agree. The main parameter which appears to affect the system differently in the simulation and continuum theory is the load force f at the filopodium tip. The agent-based model is affected by an increased force much more than the continuum mean-field theory, and filopodium growth at large force is overestimated in the latter theory. Although it is natural to attribute the discrepancy to neglect of fluctuations in the mean-field theory, it is not directly obvious how this actually occurs. We will investigate it further in the next subsection.

3.2. Breakdown of mean-field theory at large load

We now examine in more detail the reasons for the quantitative inaccuracies of the mean-field approach. The discrepancies at low values of N can be understood as being due to the fluctuations in the actin monomer concentration at the tip, which are incorporated in the agent-based simulations but are absent in the continuum equations. However, this cannot be the reason for the breakdown we observed at large load (figure 3), as fluctuations should not depend dramatically on the force applied to the membrane and limiting filopodium growth.

To explore this issue further, we have performed simulations in which the dynamics of monomeric actin is not explicitly included, instead it is always taken to be at the bulk concentration, c_0. Therefore, the growth law of the filopodium length, $L(t)$, in the mean-field approximation used above obeys a simpler equation, namely

$$\frac{\partial L}{\partial t} = \delta[k_{on}c_0\,e^{-\beta f\delta/N} - k_{off}] - v_{retr}. \qquad (10)$$

The agent-based simulation is run with $N = 30$ actin filaments, each of which can polymerize at rate $k_{on}c_0$ and depolymerize at rate $k_{off} = k_{on}c_0/100$. We disregard retrograde flow, and initialise the filaments with a displacement along their direction equal to δ/N between each other—this is to avoid the locking problem mentioned in section 2.1. The comparison between the simulation results and equation (10) in figure 5 clearly shows that the discrepancy is already there at the level of a simulation which disregards any fluctuation in the local monomeric actin concentration. The breakdown is instead due to the approximation that having a bundle of N fibres, as opposed to a single fibre, can be simply taken into account by setting $k_{on} \rightarrow k_{on}N$ in the single fibre equation, as this assumes that all fibres have the same chance of polymerizing. While not a bad assumption for small f, this approximation breaks down dramatically for large f, as the filaments essentially grow one at a time. This is because the fibre farthest from the membrane is by far the most likely to elongate by exploiting a gap which appears due to membrane diffusion. Consequently, the polymerization events in the dynamics are highly correlated and the mean-field approximation breaks down.

3.3. Filopodia growth in the presence of motors: parameter choices

From the numerical results in section 3.1 and figure 4, we can see that for the realistic values of parameters the maximal
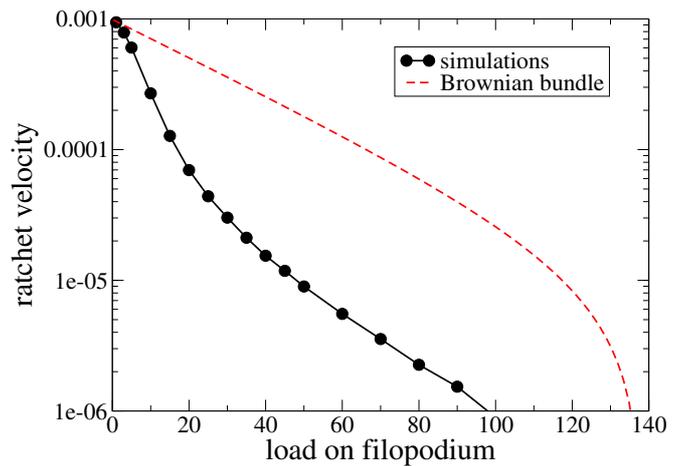

Figure 5. Comparison between the mean-field prediction (dashed lines) and simulations (points) for the velocity of a bundle of Brownian ratchet, for $v_{retr} = 0$ and $k_{on}c_0/k_{off} = 100$. It can be seen that the mean field significantly overestimates the numerical data. Data are shown in simulation units: one force unit corresponds to about 1.5 pN.

length that can be supported by this diffusion-limited process is quite small, even when neglecting the effect of fluctuations which, as we showed in section 3.2, further limit the steady-state length of the filopodium. There must therefore be another mechanism that allows the filopodia to reach lengths as large as 40 μm [11]. One possibility, that we explore in this section, is that larger lengths are made possible via the directed transport of actin monomers by myosin motors [16, 17], which have been associated with filopodia growth for a long time [35–37]. Whereas a long bundle will have to wait a significant amount of time for an actin monomer to reach the tip by diffusion alone, it might be possible that the advective transport process will be much faster.

First we discuss the choice of parameters that we make to study filopodial growth with motors. In particular, we have considerable freedom in choosing the attachment and detachment rates (k_a and k_d respectively). In what follows, we for simplicity ensure (unless specified otherwise) that $Nk_a = k_d$ so that $c_d \sim c_a$ at the filopodial base, which is reasonable given the recent experimental data [38]. Note that in [16], the authors consider a very large range of $k_d = 1$–$3000\ s^{-1}$, but as we will see below, we require much smaller values of k_d in order to allow motors to aid filopodial growth. The remaining key parameter in the advection simulation is the motor advection, v. Myosin X is known to be a highly processive motor, however the details of its interactions with G-actin are poorly understood [16]. Here we will present results with a value of v, in the μm s^{-1} range, which is at the high end of the biologically relevant range [16].

In the following section, we analyse the numerical results obtained by considering myosin-aided advection in our mean-field theory in equations (1)–(3).

3.4. Filopodia growth in the presence of motors

We now discuss the filopodium dynamics predicted by equations (1) and (3), when motor-induced transport is included.
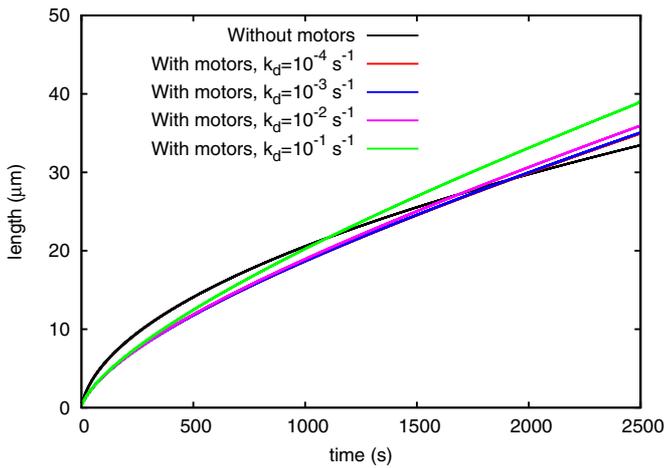
Figure 6. Filopodium length as a function of time from numerical integration of equations (1)–(3). Initially, adding myosin motors slows down filopodial growth, see discussion in the text. Simulation parameters are $N = 10$, $f = 10$ pN, $k_{off} = 1$ s^{-1}, $k_{on} = 10$ μM^{-1}s^{-1}, $a_0 = 10$ μM and advection velocity $v = 0.5$ μm s^{-1}.

In analogy with the presentation of the results in section 3.1, we first consider the (physically unrealistic) case in which there is *no* retrograde flow (parameters not discussed below are set according to table 1). Figure 6 compares growth dynamics of a filopodium (made of $N = 10$ fibres) in the absence and presence of myosin-mediated transport; while figure S2 (available at stacks.iop.org/PhysBio/11/016005/mmedia) shows some typical corresponding density profiles of diffusing and advected monomers. When motors are included the initial growth rate of the filopodium is actually slower. Although this result may at first sight seem surprising, it is consistent with the findings of [15], which studied a similar system with a spatial Gillespie algorithm. The reason for such a behaviour can be appreciated by comparing the initial growth rate coming from diffusion and motor advection respectively. The former can be estimated as (parameters as in figure 6)

$$[k_{on}c_0 \, e^{-\beta f\delta/N} - k_{off}]\delta \sim 137 \, \text{nm s}^{-1}. \tag{11}$$

The latter, the initial growth rate when considering also advection, can be estimated as

$$\left[k_{on}c_d(0) \, e^{-\beta f\delta/N} + \frac{vc_a(0) \, e^{-\beta f\delta/N}\eta}{N} - k_{off}\right]\delta \sim 74 \, \text{nm s}^{-1}. \tag{12}$$

Therefore, paradoxically, sequestration of G-actin monomers by myosin X motors advecting along the actin bundle initially *slows down* rather than accelerates the length growth.

By using this argument, it is straightforward to find a criterion on the parameters for the filopodium to initially grow faster with advection. For this to be the case, one requires:

$$k_{on}c_d(0) + \frac{vc_a(0)\eta}{N} > k_{on}c_0. \tag{13}$$

Using the boundary conditions (equations (4)–(6)), and re-arranging the terms, we can find that this condition is linked to the value of the following dimensionless number:

$$\lambda = \frac{v\eta}{Nk_{on}}. \tag{14}$$

If $\lambda > 1$, the initial growth will be greater with motors. Using values in table 1, we find that $\lambda = 1$ requires $v \sim 5$ μm s^{-1}, which is unlikely for myosin X advection. We should stress that, while equation (12) holds in general, equation (13) exploits the assumption that $c_a(0) + c_d(0) = c_0$, as used previously in in [15]. A different boundary condition at the base of the filopodium may therefore affect our conclusion. In particular using $c_d(0) = c_0$ and taking $c_a(0)$ proportional to the number of filaments N leads to an enhancement of the growth rate by motor advection (see figure S3 available at stacks.iop.org/PhysBio/11/016005/mmedia, where the same value of v used in figure 6 is used). However, as mentioned when introducing our continuum model, this assumption would require the G-actin concentration to be several-fold larger than in the bulk, a hypothesis for which there is no clear evidence to date[10].

In the absence of retrograde flow, as noted also in section 3.1, there can be no steady state. Under this condition advection eventually leads to longer filopodia, as it yields linear growth if $c_a(L) \neq 0$, as opposed to $L(t) \sim t^{1/2}$ when diffusion is the only transport mechanism. However, as is apparent from figure 6, the crossover between diffusion-dominated and advection-dominated growth occurs for unrealistically high values of the filopodial length (around 20 μm in figure 6, even though a rather large advection velocity, $v = 0.5$ μm s^{-1}, is assumed). These lengths are likely to be irrelevant for filopodia *in vivo*, as elasticity would halt the growth much sooner.

Also when v_{retr} is non-zero, and a steady state can be reached, the size and growth rate of filopodia are not significantly enhanced by motor transport for $v = 0.5$ μm s^{-1} (see figure 7). For small values of λ and of the kinetic constants k_a and k_d filopodia grow longer with diffusional transport alone, even at late times. On the other hand, advection eventually leads to longer bundles when $k_d = Nk_a$ is larger (e.g. 0.1 s^{-1}, see figure 7). Increasing λ does lead to a dramatic difference in the kinetics, however, as previously mentioned, this would imply that motors move at unrealistically high speed.

Figures 6 and 7 strongly suggest that, with a realistic choice of parameters (see table 1), G-actin advection by myosin X hinders, rather than enhances, filopodial growth. It is, however, possible that the diffusion constant $D = 5$ μm^2 s^{-1} has been overestimated in the literature, where *in vitro* experiments might not account for the level of macromolecular crowding occurring *in vivo* [39]. If this were the case, advection might become more relevant. In figure 8, we see that with $D = 0.5$ μm^2 s^{-1} and a small detachment rate $k_d = 10^{-4}$ s^{-1}, the system with advection takes over before $L \sim 3$ μm. This represents an almost ten-fold decrease in the crossover point from the previous case when $D = 5$ μm^2 s^{-1}, and shows that given the right parameters, it might be possible for the myosin motors to have a positive effect on filopodial growth.

---

[10] We note here that even if $c_a(0)\eta$ approaches the jamming density on the bundle (equal to about one transported G-actin monomer every 5 nm in each filament), advection leads to an initial greater flux with respect to diffusion for an advection velocity of $v > 0.5$ μm s^{-1} (as in figures 6 and S3). This is still a very large value if we consider the fact that the association between G-actin and myosin X motors may be reversible [16].
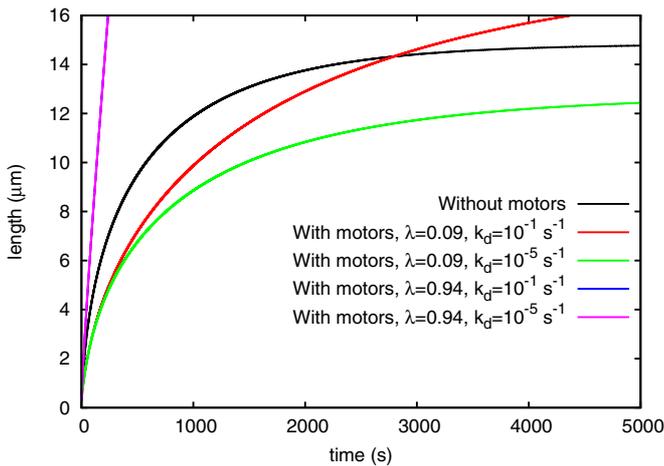
Figure 7. Filopodium length as a function of time from numerical integration of equations (1)–(3). With $v_{\text{retr}} = 15$ nm s^{-1}, the system can reach a steady state. In general, including myosin transport results in a shorter steady-state length. We show two extreme values of $k_d = 10^{-1}, 10^{-5}$ s^{-1} for $\lambda = 0.09, 0.94$ in green, red and magenta, blue respectively. If λ is sufficiently large, k_d has little effect at least in the physiological range of filopodial length. If λ is small, the strength of attachment/detachment dictates whether or not steady state is reached at all. Simulation parameters are $N = 10$, $f = 10$ pN, $k_{\text{off}} = 1$ s^{-1}, $a_0 = 10$ μM, $v = 0.5$, 5 μm s^{-1}.
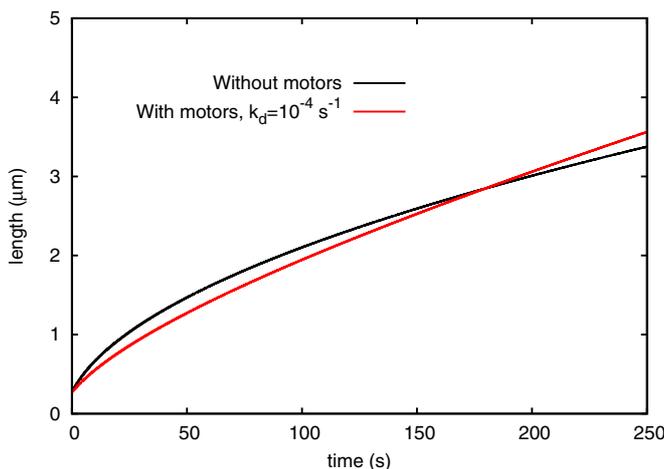

Figure 8. Filopodium length as a function of time from numerical integration of equations (1)–(3). Reducing the diffusion constant to $D = 0.5$ μm^2 s^{-1} can make the myosin motors much more relevant as the crossover point is now below $L \sim 3$ μm. Simulation parameters are $N = 10$, $f = 10$ pN, $k_{\text{off}} = 1$ s^{-1}, $a_0 = 10$ μM, $v = 0.5$ μm s^{-1}.

4. Conclusions

In conclusion, we have presented a systematic study of the growth of filopodia both in the absence and in the presence of active transport of actin monomers by myosin motors. We have compared the predictions of a set of continuum partial differential equations based on a mean-field approximation to direct simulations of an agent-based description resolving the position of each of the fibres, of the top membrane limiting the filopodium, and of monomeric actin diffusion/advection within the filopodium.

Our main results may be summarized as follows.

First, we found that the mean-field theory and the agent-based simulations are in general, qualitative agreement, but we highlighted some significant quantitative discrepancies, either for small bundles or for large forces acting on the filopodium tip. The former observation is expected, and is simply due to the neglect of fluctuations in the mean-field theory; a similar effect has also been noted in [16]. The latter discrepancy has a different origin, and we have shown that it appears even in a model considering a well-stirred environment in which depletion of G-actin monomers is not taken into account (section 3.2). We have demonstrated that the mean-field theory for bundles under a high opposing force breaks down. This is because the continuum model does not account for the fact that in the microscopic description fibres elongate one at a time i.e. essentially it is only the fibre end farthest from the membrane which elongates when a sufficiently large gap appears. To the best of our knowledge, this shortcoming of the mean-field theory had not previously been identified, in spite of the widespread use of the ratchet equation (3) to describe the growth of filopodia [11, 12, 14].

Second, we found that, surprisingly, with parameter values taken from the recent literature, myosin-directed transport of actin monomers does not effect an increase in the growth rate and steady-state length of filopodia. This can be rationalized quite simply on the basis of some order-of-magnitude estimates, from which it appears that, given the accepted values of actin diffusion, polymerization rate and myosin X velocity, the rate of advection-driven growth is notably smaller than that of diffusion-driven growth (unless the filopodium is unrealistically long). However, if we assume that crowding and confinement within the filopodial tip lead to a smaller diffusion coefficient for actin monomers, then motors *could* play a role, and lead to more efficient growth of filopodial protrusions. Furthermore, advection would also become much more relevant if it turned out that the total density of G-actin, including both diffusing and bound monomers, were much larger than the bulk intracellular concentration of actin monomers. It would be interesting to probe this possibility experimentally in the future.

We stress that our results in no way imply that myosin X transport is in general irrelevant for the physics of filopodia. On the contrary, it may well be that motor-driven transport is necessary for molecules, such as VASP, which are involved in the maintenance of the filopodial bundle [10]; we have simply found that motors are unlikely to provide a mechanism for actin monomer transport.

We hope that our results will spur further experimental investigations of cellular filopodia and their dynamics.

References

[1] Bray D 2001 *Cell Movements: From Molecules to Motility* 2nd edn (New York: Garland Publishing)
[2] Lauffenburger D A and Horwitz A F 1996 *Cell* **84** 359
[3] Peskin C S, Odell G M and Oster G F 1993 *Biophys. J.* **65** 316
[4] Burridge K, Fath K, Kelly T, Nuckolls G and Turner C 1988 *Annu. Rev. Cell Biol.* **4** 487
[5] Hawkins R J, Poincloux R, Benichou O, Piel M, Chavrier P and Voituriez R 2011 *Biophys. J.* **101** 1041

[6] Poincloux R, Collin O, Lizarraga F, Romao M, Debray M, Piel M and Chavrier P 2011 *Proc. Natl Acad. Sci. USA* **108** 1943

[7] Tjhung E, Marenduzzo D and Cates M E 2012 *Proc. Natl Acad. Sci. USA* **109** 12381

[8] Svitkina T M and Borisy G G 1999 *J. Cell Biol.* **145** 1009

[9] Svitkina T M, Chaga O Y, Vignjevic D M, Kojima S, Vasiliev J M and Borisy G G 2003 *J. Cell Biol.* **160** 409

[10] Mejillano M R, Kojima S, Applewhite D A, Gertler F B, Svitkina T M and Borisy G G 2004 *Cell* **118** 363

[11] Mogilner A and Rubinstein B 2005 *Biophys. J.* **89** 782–95

[12] Daniels D R 2010 *Biophys. J.* **98** 1139

[13] Daniels D R 2008 *Phys. Rev. Lett.* **100** 048103

[14] Daniels D R, Marenduzzo D and Turner M S 2006 *Phys. Rev. Lett.* **97** 098101

[15] Zhuravlev P I, Der B S and Papoian G A 2010 *Biophys. J.* **98** 1439–48

[16] Lan Y and Papoian G A 2008 *Biophys. J.* **94** 3839

[17] Zhuravlev P I, Lan Y, Minakova M S and Papoian G A 2012 *Proc. Natl Acad. Sci. USA* **109** 10849

[18] Zhuravlev P I and Papoian G A 2011 *Cell Adhes. Migration* **5** 448

[19] Zhuravlev P I and Papoian G A 2009 *Proc. Natl Acad. Sci. USA* **106** 11570

[20] Ott A, Magnasco M, Simon A and Libchaber A 1993 *Phys. Rev. E* **48** R1642

[21] Sanz E and Marenduzzo D 2010 *J. Chem. Phys.* **132** 194102

[22] Andrews S S and Bray D 2004 *Phys. Biol.* **1** 137

[23] Press W H, Teukolsky S A, Vetterling W T and Flannery B P 1992 *Numerical Recipes in C: The Art of Scientific Computing* 2nd edn (Cambridge: Cambridge University Press)

[24] Carlsson A E 2001 *Biophys. J.* **81** 1907–23

[25] Sheetz M P, Wayne D B and Pearlman A L 1992 *Cell Motil. Cytoskeleton* **22** 160–9

[26] McGrath J L, Tardy Y, Dewey C F, Meister J J and Hartwig J H 1998 *Biophys. J.* **75** 2070

[27] Pollard T D 1986 *J. Cell Biol.* **103** 2747

[28] Gardel M L, Sabass B, Ji L, Danuser G, Schwarz U S and Waterman C M 2008 *J. Cell Biol.* **6** 999

[29] Mogilner A and Oster G 1996 *Biophys. J.* **71** 3030

[30] Burroughs N J and Marenduzzo D 2005 *J. Chem. Phys.* **123** 174908

[31] Burroughs N J and Marenduzzo D 2007 *Phys. Rev. Lett.* **98** 238302

[32] Sugden K E P, Evans M R, Poon W C K and Read N D 2007 *Phys. Rev. E* **75** 031909

[33] Nowak S A, Fok P-W and Chou T 2007 *Phys. Rev. E* **76** 031135

[34] Tailleur J, Evans M R and Kafri Y 2009 *Phys. Rev. Lett.* **102** 118109

[35] Berg J S and Cheney R E 2002 *Nature Cell Biol.* **4** 246

[36] Berg J S, Powell B C and Cheney R E 2001 *Mol. Biol. Cell* **12** 780

[37] Wang F S, Wolenski J S, Cheney R E, Mooseker M S and Jay D G 1996 *Science* **273** 660

[38] Nagy S, Ricca B L, Norstrom M F, Courson D S, Brawley C M, Smithback P A and Rock R S 2008 *Proc. Natl Acad. Sci. USA* **105** 9616

[39] Ellis R J 2001 *Trends Biochem. Sci.* **26** 597